

Hubble Space Telescope

(HST)

Optics Performance Enhancement

(OPE)

Preliminary Feasibility Study

(HST10X)

An investigation of one approach to provide an 8-meter class UV/Optical Space Telescope.

Summary Report,

.pdf files

This file,

HST10X_Technical.pdf,

is one of five .pdf files for this report.

It includes the Table of Contents for the entire report

and report Section 5

Technical Reports

The other files are:

HST10X_Summary.pdf

HST10C_SCIENCE.pdf

HST10X_Mission.pdf

HSY10X_Optical.pdf

Hubble Space Telescope

(HST)

Optics Performance Enhancement

(OPE)

Preliminary Feasibility Study

(HST10X)

**An investigation of one approach
to provide an 8-meter class
UV/Optical
Space Telescope.**

Summary Report

Table of Contents

| Section | Page |
|--|-----------|
| 1. Executive Summary | 1 |
| 1.1 Overview..... | 1 |
| 1.1.1 Abstract..... | 1 |
| 1.1.2 Background..... | 1 |
| 1.1.3 Study Goal..... | 1 |
| 1.1.4 Study Teams..... | 1 |
| 1.1.5 Study Limits..... | 2 |
| 1.1.6 Study Conclusion..... | 2 |
| 1.1.7 Study Results Summary..... | 2 |
| 1.2 Science Enabled by the HST10X Enhancement..... | 3 |
| 1.3 The Installation Mission..... | 3 |
| 1.4 Optical Assessment..... | 4 |
| Figure 1.4.1 Ray-trace of the "add-on" telescope..... | 4 |
| Figure 1.4.2 The Two-fold Mirror Concept..... | 5 |
| Figure 1.4.3 The Afocal Telescope Concept..... | 5 |
| Figure 1.4.4 HST10 and Enhancement Components in the Orbiter Cargo Bay..... | 5 |
| 1.5 Technical Reports..... | 6 |
| 1.5.1 Structural Dynamics..... | 6 |
| 1.5.2 Thermal Assessment..... | 6 |
| 1.5.3 Fine Guidance Sensor Operation..... | 6 |
| 1.5.4 Pointing and Control..... | 6 |
| 1.5.4.1 Control Systems..... | 6 |
| 1.5.4.2 Orbit Decay..... | 6 |
| 1.5.5 ION Engine Stationkeeping System..... | 7 |
| 1.6 Team List..... | 7 |
| 1.7 Example Schedule..... | 7 |
| 2 Science with HST10X | 8 |
| 2.1 Introduction..... | 8 |
| 2.2 HST10X Performance..... | 9 |
| 2.2.1 Optical Performance..... | 9 |
| Table 2.1 The HST10X Afocal Telescope..... | 9 |
| Table 2.2 Comparison of Two-pixel Resolution (arc-sec) at 500 nm..... | 9 |
| Figure 2.1 An Extraction from the HDF F814W Composite image..... | 9 |
| Figure 2.2 Simulated Images of Interacting Galaxies..... | 10 |
| Table 2.3 HST10X Areal Coverage (Square Arc-minutes)..... | 10 |
| Table 2.4 HST10X Limiting Magnitudes (SNR = 10)..... | 11 |
| Table 2.5 ACS/WF2 Orbits to Equal One HST10X Orbit..... | 11 |
| 2.2.2 UV Performance..... | 11 |
| Table 2.6 HST10X Limiting Fluxes with STIS and COS..... | 11 |
| 2.3 Examples of Outstanding Science Enabled by HST10X..... | 12 |
| 2.3.1 Detection and Spectroscopy of Earth-like Planets..... | 12 |
| 2.3.2 The Formation and Evolution of Galaxies..... | 12 |
| Figure 2.3 Three Small Fields from the HDF North composite, true color image..... | 13 |
| 2.3.3 Cepheid Distances and Large Scale Flows within 100 Mpc..... | 13 |
| 2.3.4 Origin of Stellar and Planetary Systems..... | 14 |
| Figure 2.4 Protoplanetary Disks in Orion..... | 14 |
| 2.3.5 Observational programs that will be carried out with HST10X-WFC3/ ACS will include:..... | 15 |
| 2.3.6 Large Scale Structure..... | 15 |
| Figure 2.5 Large-scale Cosmological Structure..... | 16 |
| Table 2.7 Quasar Number Counts and Mean Angular Distance..... | 17 |
| 3. Cargo/Installation Mission System Description | 18 |
| 3.1 Mirror Configuration for the Cargo Bay..... | 18 |
| 3.2 Installation Mission Overview..... | 18 |
| 3.3 Cargo Elements..... | 18 |
| 3.3.1 Orbital Replacement Unit (ORU) Description..... | 18 |
| 3.3.2 Space Support Equipment (SSE)..... | 20 |
| 3.4 Mission Sequence Description..... | 22 |
| 3.4.1 EVA Day 1, Remove OLS and Install Ion Thrusters..... | 22 |
| 3.4.2 EVA Day 2, Install New Light Shield, but do not Deploy Axially..... | 22 |
| 3.4.3 EVA Day 3, Prepare and Install New Mirror Assembly..... | 22 |
| 3.4.4 EVA Day 4, Swap SI's..... | 23 |
| 3.4.5 Deploy HST..... | 23 |
| 3.5 Flight System & Servicing Remaining Issues..... | 23 |
| 3.6 Mission Sequence Pictorial..... | 24 |

| | |
|--|-----------|
| 4. Optical Assessment | 25 |
| 4.1 Introduction | 25 |
| 4.2 Mirror Design Selection | 25 |
| Figure 4.1 Ray-trace of "add-on" telescope | 26 |
| 4.3 Optical Assessment Overview | 26 |
| Figure 4.2 The Afocal "add-on" Telescope Concept | 26 |
| Figure 4.3 The Two-fold Mirror Concept | 27 |
| Table 4.1 VLT Blank Parameters | 27 |
| 4.4 Attachment to existing structures | 27 |
| 4.5 Optical Parameters | 28 |
| 4.5.1 General Characteristics of Afocal Approach | 28 |
| Table 4.5.1 Telescope Assembly Optical Parameters | 28 |
| Table 4.5.2 Telescope Alignment Error Summary | 29 |
| Table 4.5.3 LOS Control Error Budget | 29 |
| Table 4.5.4 Wavefront Error Budget for Currently Planned SIs | 30 |
| 4.5.2 Conclusions from the Error Budgets | 30 |
| 4.6 HST10X to SI Interface is Retained | 31 |
| 4.7 Science Instrument Complement | 31 |
| Table 4.7.1 SI Complement | 31 |
| Table 4.7.2 SI Performance Comparison | 32 |
| 4.8 To Optimize HST10X Capabilities | 33 |
| Table 4.8.1 CODEX Wadsworth Spectrometer Parameters | 33 |
| Table 4.8.2 Wavefront Error Budget with CODEX Correction | 34 |
| 5. Technical Reports | 35 |
| 5.1 HST10X Structural Dynamics Assessment | 35 |
| 5.1.1 The HST10X Dynamic Model | 35 |
| 5.1.2 HST10X Primary and Secondary Mirror Assemblies | 35 |
| 5.1.3 HST10X Light-Shield Assembly | 36 |
| 5.1.4 The HST10X-HST Modeled System | 36 |
| Table 5.1.1 HST10X Mass Properties | 37 |
| Table 5.1.2 Properties of ABLE Booms | 37 |
| Table 5.1.3 Equations for Modal Gains | 37 |
| Table 5.1.4 Dynamics of the HST10X Assembled Spacecraft | 38 |
| Table 5.1.5 Dynamics of the HST10X Primary/Secondary Mirror Assembly | 39 |
| Table 5.1.6 Dynamics of the HST10X Light-Shield Assembly | 40 |
| 5.2 HST10X Preliminary Thermal Systems Assessment | 41 |
| 5.2.1 HST10X Thermal Assessment Assumptions | 41 |
| 5.2.2 AFT Shroud Impacts | 41 |
| 5.2.3 Forward Section Assessment | 41 |
| 5.2.4 Conclusions | 42 |
| 5.3 FGS Impacts from HST10X Enhancement | 42 |
| 5.3.1 Optical Configuration Considered | 42 |
| 5.3.2 Reduction in the FGS field of view (FOV) | 42 |
| 5.3.3 Guide Star Acquisitions | 42 |
| 5.3.4 Jitter and the PCS/FGS system | 43 |
| 5.4 Pointing and Control | 43 |
| 5.4.1 Slew and Control System Performance | 43 |
| 5.4.2 Accelerated Orbit Decay | 43 |
| 5.5 Mission Analysis for an HST10X Ion Engine Stationkeeping System | 44 |
| 5.5.1 Stationkeeping Analysis Issues | 44 |
| 5.5.2 Stationkeeping System Design | 44 |
| 5.5.3 Stationkeeping System Description | 45 |
| Figure 5.5 IESS Configuration | 45 |
| 6. HST10X Study Team | 46 |
| 6.1 Study Manager | 46 |
| 6.2 Science Team Leads | 46 |
| 6.3 Design Engineering Team | 46 |
| 6.3.1 Lockheed Martin | 46 |
| 6.3.2 Swales | 46 |
| 6.3.3 University of Arizona | 46 |
| 6.3.4 Raytheon Optical Systems | 46 |
| 6.3.5 Ball Aerospace | 46 |
| 6.3.6 Orbital Science Corp. | 46 |
| 7. HST10X Example Schedule | 47 |
| 7.1 HST10X Example Schedule sheets 1 and 2 of 3 | 47 |
| 7.2 HST10X Example Schedule sheet 3 of 3 | 48 |

5. Technical Reports

5.1 HST10X Structural Dynamics Assessment

The HST10X Structural Dynamics Assessment was conducted to investigate the mass properties, interaction with the Pointing Control System, thermal deformation, and potential line-of-sight jitter of the Hubble Space Telescope with the HST10X enhancement. The dynamic mathematical model of HST developed after the first servicing mission (SM-1), was modified with added large mirrors and light-shield to approximate the properties of an example HST10X configuration.

Conclusions: The increased Moment-of-Inertia (MOI) will require increased slew times and more reaction-wheel torque but within acceptable margins, light-shield resonance may require minor changes to the control law, pointing jitter can be mitigated with the line-of-sight control of the secondary mirror if necessary, and the enhancement will add about approximately 3,500 pounds to the current HST weight budget of approximately 24,000 pounds which is about 15%.

The (MOI) will approximately double which will slow slews and require more reaction wheel momentum. The only significant resonance mode seems to be the light-shield up around 4 to 6 Hz which may require some control law changes. We can stand considerable jitter in the primary control system if we create a 10 Hz Line-of-Sight (LOS) control loop on the Secondary Mirror. Because the New Secondary Mirror (NSM) is so light (Small MOI), this loop should have almost no effect on the Primary loop.

A technical description of the model and results produced by it follow.

5.1.1 The HST10X Dynamic Model

The dynamic model of the HST was produced following the first Service Mission 1 (SM-1). It is in the form of mode shapes, natural frequencies, and damping. Several modifications were done to make it suitable for the HST10X enhancement. First, the modes from the Solar Array 2 (SA-2) were removed below 0.6 Hz. Above this frequency, coupling of the modes made it too difficult to identify individual modes of the SA-2 alone. The mass and moment

of inertia of SA-2 could not be extracted without causing instabilities in the model, so it was left. Hence, the HST model is overweight by about 710 lb which is acceptable at this coarse level of simulation. Next, the Aperture Door (AD) and the forward 3.5-m section of the existing Light-Shield Assembly (LSA) were removed. This was done by eliminating the AD mode at 0.9 Hz and rigid body mass subtraction of 520 lb for the LSA and 105 lb for the AD.

Then, new parts were added to bring the model up to its current condition. This included addition of the Solar Array-3 (SA-3) wings (in their 0° orientation), the cooling system equipment Electronics Support Module (ESM) and NICMOS CryoCooler (NCC), and radiators for the NICMOS Cooling System (NCS) and Aft Shroud Cooling System (ASCS). This added over 2,547 lb to the aft bulkhead and aft shroud of the System Support Module (SSM). The resulting mass properties are shown in Table 5.1.1.

5.1.2 HST10X Primary and Secondary Mirror Assemblies

The example HST10X primary mirror is modeled as a thin mirror surface supported on actuators that are fixed to a contoured shell support structure. The mirror (2 mm thick) and light-weight actuators (50 per m²) are modeled as non-structural mass at 5.0 kg/m². The shell is 5" thick aluminum-core honeycomb with 0.060" Glass/Epoxy (G/E) face sheets. This thickness provides enough lamina to develop a minimum Coefficient-of-Thermal Expansion (CTE) structure, and is light weight and stiff. By careful design, the actual CTE can be kept to about $2 \times 10^{-7} / ^\circ\text{C}$ or lower. Radial stiffeners connect the shell to a central stiff ring. This ring is attached to the existing Optical Telescope Assembly (OTA) metering truss at four points modeled as ball joints. The New Primary Mirror (NPM) is modeled as hinged at two places to fit in the Orbiter cargo bay. It is assumed that the backup structure is tightly bolted along these hinge lines when deployed to eliminate slop and dead-band. The honeycomb plate, however, is modeled as discontinuous at the hinge lines.

A mast locates the New Secondary Mirror (NSM) relative to the primary. The mast of G/E is a 25" OD tube with 0.50" wall. Radial gussets connect it to the primary mirror structure. The four gussets are 0.65" thick in order to match the shading caused by the existing OTA secondary-mirror spider. They extend only part way up the mast because of packaging constraints when stowed in the Orbiter cargo bay. At some section, a bolted joint is assumed that is open when stowed. Otherwise, the mast is a single-piece structure without joints or subassemblies.

The New Secondary Mirror assembly, like the primary, is a thin mirror surface supported on about 230 small actuators that connect to a contoured honeycomb-plate. The mirror and actuators are modeled as 5.0 kg/m² non-structural mass. A 50 lb lump is included to account for a yet to be designed sun blocking mechanism to serve as an aperture door. The honeycomb is 3" thick with 0.060" G/E face sheets and aluminum core. Six radial stiffeners connect it to the central mast.

Properties of the combined new primary-secondary assembly are shown in Table 5.1.1 for the mass, and Table 5.1.4 for the structural dynamics. Here, as elsewhere, modal damping of 0.5% of critical is assumed. Weight contingency of 20% is used on the structural mass portion. This is expected to be reasonably conservative.

5.1.3 HST10X Light-Shield Assembly

The HST10X New Light-Shield (NLS) is modeled as made entirely of deployable ABLE booms and Multi-Layer Insulation (MLI) blankets. In the model, three booms span out from a stiff central ring to the 9-m outer diameter at eight equally spaced locations. The central ring connects to the System Support Module (SSM) Forward Shell with four ball joints. Then, eight booms extend in the axial (V1 or X) direction for nine meters to support the light shield. The seven layer MLI (0.07 lb/ft²) covering is loosely connected so that its thermal deformation is largely de-coupled from the booms. The ABLE booms are standard items with beam-like properties. These properties are shown in Table 5.1.2

The modeled structural dynamic properties of the Light-Shield Assembly are listed in Table

5.1.6. It shows the first natural frequency is at only 0.166 Hz. A set of major interactive modes begins at about 1 Hz. Because of symmetry of bending, the first five modes have no coupling to the base point, as evidenced by their modal effective weight values of zero.

5.1.4 The HST10X-HST Modeled System

The subassemblies were combined by standard techniques. The HST10X primary/secondary mirror assembly in Craig-Bampton form was coupled to the OTA metering truss forward ring (at station 450.65), and the HST10X light-shield, also in Craig-Bampton form, was coupled to the SSM forward shell (at station 455.30). Since the HST (SSM and OTA) model was in the form of free system modes shapes, 564 modes were used up to 100 Hz to ensure convergence.

The free system was computed for 260 vibration modes to 16 Hz. The modal gains were calculated from this system. There are two types of gains of interest, one for the line-of-sight and one for the rate-gyro assemblies. For the line-of-sight, a ray trace equation was used that included the HST10X NPM and NSM, and the OTA Primary Mirror (PM) and Secondary Mirror (SM), and terminated at the OTA focal point. Because the HST10X mirrors are flexible, a paraboloid of revolution was fitted to their deformed shapes to determine the best-fit least-squares displacement in translation and rotation. The equations for the two modal gains, called K_B , are shown in Table 5.1.3

The natural frequencies and modal gains of the assembled system are listed in Table 5.1.4. This data is for the solar arrays in their 0° orientations. Time precludes studying other orientations. The first six modes are for the free system as a rigid body which, by definition, have modal gains that sum to unity. The other modes are for elastic motion. Only the few modes with significant gains are listed. Above six Hz the table has been truncated because it is the low frequency modes that are of most concern to the control system. Modal damping is assumed to be 0.5% of critical. Unfortunately, because of the nature of the models, there are no plots of the system mode shapes. Other than the mass contingency, no uncertainty factors have been applied to these results.

| Subassembly | Structural Mass (kg) | Non-Structural Mass (kg) | Total Mass (kg) | M. O. I. at the Center-of-Mass | | |
|---|----------------------|--------------------------|-----------------|--------------------------------------|--------------------------------------|--------------------------------------|
| | | | | I ₁₁ (kg-m ²) | I ₂₂ (kg-m ²) | I ₃₃ (kg-m ²) |
| HST10X Primary-Mirror Assembly | 1537 | 240 | 1777 | 11,400 | 6,300 | 5,300 |
| HST10X Secondary-Mirror Assembly with Mast | 727 | 21 | 748 | 150 | 11,000 | 11,000 |
| HST10X Light-Shield Assembly | 291 | 257 | 548 | 8,900 | 11,000 | 11,000 |
| HST10X w/o AD, Fwd. Shell, or SA-2 with SA-3, NCS, and ASCS | | | 12054 | 51,000 | 77,000 | 90,000 |
| System Total | | | 15127 | 73,200 | 204,000 | 216,000 |

Table 5.1.1 HST10X Mass Properties

| | | |
|-----------------|----------------------------------|--|
| Construction | solid, circular S-G/E longerons, | 10" outside radius |
| Boom weight | 0.0477 lb/in | EA = 4.77x10 ⁶ lb-in ² |
| Canister weight | 51.0 lb each | EI = 79.5x10 ⁶ lb-in ² |
| | | GJ = 5.0x10 ⁶ lb-in ² |

The units of pounds and inches are shown to match the supplier's catalogues.

Table 5.1.2 Properties of ABLE Booms

$$K_{B_{ii}}^{LOS} = I_{ii} \theta_{LOS i} \theta_{RWA i} / m$$

and

$$K_{B_{ii}}^{RGA} = I_{ii} \theta_{RGA i} \theta_{RWA i} / m$$

where:

i = 1, 2, or 3 for axis V1, V2 or V3

I_{ii} = the center-of-mass moment of inertia of the system about axis i, (kgm²)

θ_{RWA} = modal rotation of the Reaction Wheel Assemblies on the HST SSM, (rad)

θ_{LOS} = modal rotation of the system line-of-sight from a ray trace equation, (rad)

θ_{RGA} = modal rotation of the Rate Gyro Assembly on the OTA equipment shelf, (rad)

m = generalized mass of the mode shape (kg-m²).

Table 5.1.3 Equations for Modal Gains

| Mode Nr. | Nat. Freq. (Hz) | Modal Gains for Line-of-Sight | | | Modal Gain for the RGAs | | |
|-------------|---------------------------|-------------------------------|------------------|------------------|-------------------------|------------------|------------------|
| | | $K_B^{LOS}_{11}$ | $K_B^{LOS}_{22}$ | $K_B^{LOS}_{33}$ | $K_B^{RGA}_{11}$ | $K_B^{RGA}_{22}$ | $K_B^{RGA}_{33}$ |
| 1-6 | 0.00 | 1.000 | 1.000 | 1.000 | 1.000 | 1.000 | 1.000 |
| 13-14 | 0.30 | 0 | .007 | .006 | 0 | .007 | .006 |
| 29 | 0.31 | .005 | 0 | 0 | .005 | 0 | 0 |
| 32-33 | 0.46 | 0 | .131 | .114 | 0 | .134 | .114 |
| 34 | 0.59 | .161 | 0 | 0 | .161 | 0 | 0 |
| 69-71 | 0.95 | .029 | .005 | .010 | .029 | .007 | .014 |
| 76-78 | 1.20 | .214 | .003 | .039 | .213 | .001 | .014 |
| 80-81 | 1.35 | .005 | .509 | .516 | .005 | .274 | .296 |
| 96-98 | 2.00 | .164 | .001 | .012 | .162 | 0 | .008 |
| 111-112 | 2.49 | .006 | 0 | .035 | .006 | 0 | .024 |
| 121-122 | 2.88 | .001 | .003 | .026 | .001 | .002 | .019 |
| 133 | 3.36 | 0 | .002 | .012 | 0 | .001 | .008 |
| 141-142 | 3.95 | 0 | -.001 | -.002 | 0 | 0 | .001 |
| 144-145 | 4.07 | 0 | .019 | .023 | 0 | .025 | .033 |
| 159 | 4.86 | 0 | -.002 | -.072 | 0 | 0 | .074 |
| 163-164 | 5.24 | 0 | -.073 | .023 | 0 | .255 | .259 |
| 171-173 | 5.45 | 0 | .010 | .032 | 0 | .010 | .084 |
| 179-181 | 5.84 | .052 | 0 | -.085 | .001 | 0 | .063 |

Table 5.1.4 Dynamics of the HST10X Assembled Spacecraft with the Solar Arrays at their 0° Orientation

| □ □ □ Mode | Freq. (Hz) | Damping Ratio | Modal Effective Weights (Pct. of Total at I/F) | | | | | |
|---------------------|-------------------|----------------------|--|--------|--------|--------|--------|--------|
| | | | F1 | F2 | F3 | M1 | M2 | M3 |
| 1 | 1.2036 | 0.005 | 0 | 10.800 | 0 | 0 | 0 | 62.550 |
| 2 | 1.2039 | 0.005 | 0 | 0 | 10.797 | 0 | 59.099 | 0 |
| 3 | 1.3005 | 0.005 | 0 | 0 | 0 | .832 | 0 | 0 |
| 4 | 3.9335 | 0.005 | 0 | 0 | 0 | .903 | 0 | 0 |
| 5 | 4.0608 | 0.005 | 0 | 0 | 1.712 | 0 | .258 | 0 |
| 6 | 4.0620 | 0.005 | 0 | .978 | 0 | 0 | 0 | .148 |
| 7 | 4.0657 | 0.005 | 0 | .729 | 0 | 0 | 0 | .111 |
| 8 | 4.8115 | 0.005 | 0 | 0 | 0 | .076 | 0 | 0 |
| 9 | 5.2160 | 0.005 | .024 | 0 | 0 | 0 | 0 | 0 |
| 10 | 5.3885 | 0.005 | 0 | 0 | 0 | .002 | 0 | 0 |
| 11 | 5.4853 | 0.005 | 0 | .897 | 0 | 0 | 0 | 15.915 |
| 12 | 5.8979 | 0.005 | 0 | 0 | 1.594 | 0 | 29.667 | 0 |
| 13 | 6.1167 | 0.005 | 0 | .479 | 0 | 0 | 0 | 9.928 |
| 14 | 6.3164 | 0.005 | .001 | 0 | .049 | 0 | .360 | 0 |
| 15 | 7.6422 | 0.005 | 0 | 0 | 0 | .004 | 0 | .002 |
| 16 | 8.2320 | 0.005 | 0 | 3.648 | 0 | 0 | 0 | 2.906 |
| 17 | 8.2382 | 0.005 | .003 | 0 | 3.547 | 0 | 2.484 | 0 |
| 18 | 8.2740 | 0.005 | 31.108 | 0 | 0 | 0 | 0 | 0 |
| 19 | 9.1421 | 0.005 | 1.774 | 0 | 0 | 0 | 0 | 0 |
| 20 | 10.5334 | 0.005 | 0 | .061 | 0 | .067 | 0 | .031 |
| 21 | 10.5645 | 0.005 | 0 | 0 | .301 | 0 | .135 | 0 |
| 22 | 10.6277 | 0.005 | 0 | .110 | 0 | .005 | 0 | .056 |
| 23 | 10.8097 | 0.005 | .021 | 0 | .017 | 0 | .003 | 0 |
| 24 | 10.9353 | 0.005 | 0 | .023 | 0 | .001 | 0 | .024 |
| 25 | 11.0092 | 0.005 | 0 | .171 | 0 | .016 | 0 | .086 |
| 26 | 12.1493 | 0.005 | .225 | 0 | 0 | .001 | .001 | 0 |
| 27 | 13.4529 | 0.005 | 0 | .002 | 0 | .160 | 0 | .001 |
| 28 | 13.8085 | 0.005 | 19.708 | 0 | 0 | 0 | 0 | 0 |
| 29 | 14.0974 | 0.005 | 0 | 2.132 | 0 | .002 | 0 | .903 |
| 30 | 14.1039 | 0.005 | .001 | 0 | 2.035 | 0 | .800 | 0 |
| 31 | 14.3071 | 0.005 | 0 | 0 | 0 | 80.678 | 0 | 0 |
| 32 | 16.9359 | 0.005 | 0 | 7.222 | 0 | 0 | 0 | .030 |
| 33 | 17.0314 | 0.005 | 0 | .012 | 0 | .004 | 0 | .001 |
| 34 | 17.0387 | 0.005 | 0 | .011 | .001 | .003 | 0 | .001 |
| 35 | 17.0725 | 0.005 | 0 | 0 | 1.044 | 0 | .002 | 0 |
| 36 | 17.0982 | 0.005 | 0 | 0 | 0 | 0 | 0 | 0 |

Table 5.1.5 Dynamics of the HST10X Primary/Secondary Mirror Assembly Constrained at the Central Interface Ring

| Mode | Freq. (Hz) | Damping Ratio | Modal Effective Weights (Pct. of Total at I/F) | | | | | |
|------|---------------|------------------|--|--------|--------|--------|--------|--------|
| | | | F1 | F2 | F3 | M1 | M2 | M3 |
| 1 | .1664 | 0.005 | 0 | 0 | 0 | 0 | 0 | 0 |
| 2 | .1719 | 0.005 | 0 | 0 | 0 | 0 | 0 | 0 |
| 3 | .1719 | 0.005 | 0 | 0 | 0 | 0 | 0 | 0 |
| 4 | .2201 | 0.005 | 0 | 0 | 0 | 0 | 0 | 0 |
| 5 | .2201 | 0.005 | 0 | 0 | 0 | 0 | 0 | 0 |
| 6 | .2970 | 0.005 | 0 | .223 | .291 | 0 | 5.540 | 4.254 |
| 7 | .2970 | 0.005 | 0 | .291 | .223 | 0 | 4.254 | 5.540 |
| 8 | .2986 | 0.005 | 9.722 | 0 | 0 | 0 | 0 | 0 |
| 9 | .2988 | 0.005 | 0 | 0 | 0 | 0 | 0 | 0 |
| 10 | .2991 | 0.005 | 0 | 0 | 0 | 0 | 0 | 0 |
| 11 | .2991 | 0.005 | 0 | 0 | 0 | 0 | 0 | 0 |
| 12 | .2991 | 0.005 | 0 | 0 | 0 | 0 | 0 | 0 |
| 13 | .2994 | 0.005 | 0 | 0 | 0 | 0 | 0 | 0 |
| 14 | .2994 | 0.005 | 0 | 0 | 0 | 0 | 0 | 0 |
| 15 | .2997 | 0.005 | 0 | 0 | 0 | 0 | 0 | 0 |
| 16 | .2997 | 0.005 | 0 | 0 | 0 | 0 | 0 | 0 |
| 17 | .3004 | 0.005 | 0 | 0 | 0 | 0 | .012 | .001 |
| 18 | .3004 | 0.005 | 0 | 0 | 0 | 0 | .001 | .012 |
| 19 | .3006 | 0.005 | .025 | 0 | 0 | 0 | 0 | 0 |
| 20 | .3014 | 0.005 | 0 | 0 | 0 | 0 | 0 | 0 |
| 21 | .3014 | 0.005 | 0 | 0 | 0 | 0 | 0 | 0 |
| 22 | .4282 | 0.005 | 0 | 32.400 | .016 | 0 | .041 | 83.915 |
| 23 | .4282 | 0.005 | 0 | .016 | 32.400 | 0 | 83.915 | .041 |
| 24 | .5690 | 0.005 | 0 | 0 | 0 | 96.077 | 0 | 0 |
| 25 | .6272 | 0.005 | 0 | 0 | 0 | 0 | 0 | 0 |
| 26 | .6276 | 0.005 | 0 | .012 | .002 | 0 | 0 | .001 |
| 27 | .6276 | 0.005 | 0 | .002 | .012 | 0 | .001 | 0 |
| 28 | .6276 | 0.005 | 0 | 0 | 0 | .017 | 0 | 0 |
| 29 | .6279 | 0.005 | 0 | .035 | .010 | 0 | .001 | .002 |
| 30 | .6279 | 0.005 | 0 | .010 | .035 | 0 | .002 | .001 |
| 31 | .6283 | 0.005 | 0 | 0 | 0 | 0 | 0 | 0 |
| ... | | | | | | | | |
| 58 | 1.0868 | 0.005 | 0 | 23.591 | 3.590 | 0 | .554 | 3.641 |
| 59 | 1.0868 | 0.005 | 0 | 3.590 | 23.591 | 0 | 3.641 | .554 |

**Table 5.1.6 Dynamics of the HST10X Light-Shield Assembly
Constrained at the Central Interface Ring**

This section adapted from a report provided to the HST10X study by:
William Haile and Carlton Miller
Swales Aerospace, July 1999

5.2 HST10X Preliminary Thermal Systems Assessment

Conclusions: In general, the results of the thermal assessment are that thermal effects will be small or can be mitigated easily, with the exception of the solar arrays. The solar-array operating temperature will be elevated by about 20 degrees C due to the space-view reduction from the New Light-Shield (NLS). This can be mitigated by the addition of supplemental solar arrays on the bottom of the NLS which will, at least partially, offset this temperature rise. Adding reflective surfaces to channel the heat back into space will provide additional relief. Making the new arrays wider than currently planned will further reduce the temperature rise.

One of the thermal issues remaining to be addressed is the temperature stability of the New Primary Mirror (NPM). It is expected that most of the science will be near the ecliptic plane resulting in about 75% of normal viewing conditions directing the earth's albedo inside the NLS every orbit. The existing 2.4-m mirror is very heavy and relatively stable thermally. The NPM will be only 2 mm thick so when the earth's albedo is directed on it, at about 30% of sun energy levels, the telescope, depending on pointing, may see 3,600 watts or so; which has to go somewhere. Probably most of it will go into the NLS because the NPM will reflect most of what hits it. If we install a few hundred localized computer controlled heaters on the mirror with enough power to replace the sun's energy (maybe 400 watts total) the New Primary Mirror shouldn't move. HST10X will probably have an aperture door for safety reasons but closing and opening the extra mechanism almost every orbit is not desirable. There are coatings available that will reject the albedo wavelength and still provide good light-baffle performance in the visible. This is unlikely to solve the whole problem but will reduce its effect. In addition, if the final mirror choice is Zerodur material, extending the NLS length to 15 meters is likely to be adequate.

5.2.1 HST10X Thermal Assessment Assumptions

The radiation view-factor to space will be reduced by approximately 1% (analytical result). An increased absorbed flux of 3% is assumed. Further analysis is needed to deter-

mine the range of increased absorbed flux through the entire range of HST10X pointing.

The historical external-surface degradation is assumed through 2010. Impacts beyond 2010, although expected to be minimal, need to be addressed

It is assumed here that HST10X pointing will be limited to +V3 (i.e., HST sun angle will be no less than 90° from +V1) based on the shortened NLS of nine meters. The longer sun shield of about 15 meters to allow pointing up to 45 degrees of the sun is expected to have minimal impact on this analysis but will have to be studied.

5.2.2 AFT Shroud Impacts

The Aft Shroud uses radiation shields on the ±V2 surfaces to dissipate instrument power but the increased absorbed flux will impact the environment. The ±V3 surfaces are blanketed due to solar and earth views.

Instrument environments (including FGS and WFPC) will increase by 1°C to 1.5°C. The impact to instrument components will be on the order of 1°C. FHST temperatures will increase by 1°C. The External Cooling System Radiator temperatures will increase by less than 5°C.

5.2.3 Forward Section Assessment

There will be small temperature impacts to the System Support Module (SSM) Equipment Section (ES) Bays and OTA ES Bays. The forward sun-avoidance angle for the optics will result in warmer attitudes for the Bays, however, the bay doors are mostly insulated. The space-view factor reduction in this case is not large (near 2%).

There will be a greater temperature impact on the Solar Arrays. There will be up to 25% view of the HST10X New Light-Shield Assembly (-V1) resulting in reduced space view. This increase is estimated to be 20°C or more for the Solar Arrays for -V1 sun point. The increase will be less for Sun toward +V3.

Mast Damper temperature will increase for -V1 sun point. The anti-sun side radiator space view decrease will cause a warmer range. The +V3 High Gain Antenna TAG temperature will

also increase - the dish could be moved to the shield if this is a problem.

5.2.4 Conclusions

Thermal impacts to the aft shroud are less than 5°C.

Internal instrument environments are impacted less than 1.5°C.

SSM Equipment Bay impacts are small due to insulation, low blockage, and forward sun-point limit.

Solar-Array wing impacts are estimated at +20°C or more for some attitudes. If this remains a problem it may be further mitigated by operational restrictions.

Other external component temperatures will increase due to reflections/reduced space view.

Although HST10X will not pose any extraordinary environmental challenges, a more detailed analysis is required for the optics and structure thermal control requirements.

This section adapted from a presentation to the HST10X study by:
D. Castro and J. Piquero,
LMTO Thermal Systems, June 1999

5.3 FGS Impacts from HST10X Enhancement

This assessment was to investigate the impacts on the Fine Guidance Sensors (FGS) if the current HST were augmented with an 8-m primary mirror and a suitable secondary mirror. The issues assessed were the FGS encoder resolution for guide-star acquisition, the field-of-view reduction, and the ability to maintain fine-lock with the amplified jitter as measured by the FGS.

Conclusions: First, the FGS will still acquire its target in the usual sequence of Search, Coarse Track, and Fine Lock. Second, the FGS field of view will be reduced from 69 square arcminutes to approximately 6.3 square arcminutes, while the faint end of the guide-star candidates improves from 14.5 to 17 v-magnitudes. Third, jitter as measured by the FGS, will be amplified by a factor of 3.3 and requires additional consideration. Finally, a trade-off study of how the much improved faint guide-star capability will offset the reduced FOV needs to be addressed by the astronomy community.

5.3.1 Optical Configuration Considered

1. Two additional parabolic mirrors, an 8.0-m primary and a 2.4-m secondary.
2. The stop is the current primary mirror.
3. Entrance diameter is 8.0 m.
4. The focal length (f_1) is 9.576 m.
5. The separation of the mirrors is 6.7032 m).

Using this configuration, raytraces were generated that yield a new plate scale of 1.1

arcseconds per millimeter and a new FGS angular magnification of 191.0. For the current HST, the plate scale and FGS angular magnification are 3.58 arcseconds per millimeter and 57.3 respectively.

5.3.2 Reduction in the FGS field of view (FOV) versus acquisition of fainter guide stars

The plate scale for the new telescope, HST10X, is reduced by a factor of 3.3. As a direct consequence, the FGS FOV will be reduced from 69 square arcminutes to 6.3 square arcminutes. Although the FOV decreases, the light collecting characteristics of the larger telescope allows the FGS to acquire 17 mv guide stars, 2.5 mv dimmer than present operations.

5.3.3 Guide Star Acquisitions

The increased angular magnification of the FGS results in a narrower S-curve. The distance between the peak and valley of the current S-curve is approximately 40 milliarcseconds (mas). With HST10X, this distance becomes 12 mas; this is an extremely narrow S-curve for this application. There was concern, initially, that the uplinkable parameter, KD, the Fine-Lock step size could not be made small enough to acquire either the peak or the valley of the S-curve. However, parameters like the FGS walk down step size will also be reduced by the 3.3 factor. The number of LSB's that it takes to generate a 6.5 mas step size for the current HST/FGS system will result in a KD of approximately 2 mas in HST10X. Hence, the

instantaneous FOV of the FGS can move in small enough increments to ensure that the Fine Lock acquisition algorithm will be successful. Using the same argument, Search and Coarse Track modes will also operate with the HST10X. While the FGS's will work with the HST10X, it is likely that K-factors and Port 1 commands will require calibration for the new system.

5.3.4 Jitter and the PCS/FGS system.

FGS guide-star acquisitions will succeed with HST10X, however, vehicle jitter will be amplified by a factor of 3.3 when observed with HST10X and the FGS's. This item will require additional study by Science, FGS, and PCS specialists.

This section adapted from a memo provided to the HST10X study by:
L. Abramowicz-Reed,
Raytheon, June 1999.

5.4 Pointing and Control

5.4.1 Slew and Control System Performance

Conclusions: For HST10X, it appears the control system will provide acceptable science and slew performance with minor changes to the controller.

The Moment-of-Inertia (MOI) increase of approximately a factor of two will increase the torque required of the control system proportionally. Because the Reaction-Wheel torque is fixed, control bandwidth must be decreased by one over the square root of the MOI change. This will increase response time and slow maneuvers. The requirement to slew 90 degrees in 18 minutes will have to be relaxed unless actuator torque can be increased.

With the New Secondary Mirror steerable, and only moving the 2-mm thick mirror surface weighing only about 50 Lbs. instead of the full 350 Lbs. Secondary Mirror Assemble, the ratio between the moving mirror and HST10X is of the order of 1000 to 1 so with 100 mas of jitter, HST10X would only react by 0.1 mas. HST's current normal rms jitter is 3.5 mas or better. The existing control law may have to be modified to suppress any new flex modes.

The increased inertia will also require an increased Bright-Object Detection (BOD) angle and/or decrease of the maximum slew rate. This operating restriction can be addressed by installing new Bright Object Detectors to provide continuous bright object coverage.

The Gravity Gradient Torque will increase by a factor of four and Aerodynamic Drag Torque by 10. These and the MOI shift will result in generally higher Reaction Wheel Assembly

(RWA) speeds. This is likely to not be a problem since HST operates the RWA's far below their rated conditions but this should be analyzed more closely. And finally, the Momentum Management System (magnetic torquer bars) may require upgrading.

5.4.2 Accelerated Orbit Decay

Conclusions: The larger New Light-Shield (NLS) and the solar maximum in 2010 combine to accelerate the rate of orbit decay to the extent that either stationkeeping or a re-boost mission will be required. An Ion-Engine Stationkeeping system is described in Section 5.5.

The minimum science floor altitude coupled with the maximum density (minimum altitude) allowable for a 90 degree slew in 50 minutes require that something must be done to keep HST above approximately 300 nautical miles altitude out beyond year 2012. One option is adding an Ion-Engine Stationkeeping System (IESS) and, aside from the added solar array power needed, this appears to be a reasonable solution for the problem. To accommodate the power required for the IESS, a combination of turning off unneeded systems to minimize power and adding solar arrays to the New Light-Shield should provide adequate power margin for the 4,500 watts required to operate the ion thrusters. It is prudent to add solar arrays to the New Light-Shield anyway because of the increased operating temperature so this should provide adequate power for intermittent boosting, approximately 10 days per year.

This section adapted from a report provided to the HST10X study by:
W. Meyer, Swales Aerospace, July 1999

5.5 Mission Analysis for an HST10X Ion Engine Stationkeeping System

Conclusions: There is a readily available Stationkeeping System that can provide sufficient boost for stationkeeping, acceptable science efficiency versus boosting ratio, and adequate fuel margin for end-of-life ascent. And, there are convenient attachment points that are structurally acceptable. There are large diameter threaded holes in the existing HST trunnion sockets that will make ideal mechanical mounts for the ion thrusters

5.5.1 Stationkeeping Analysis Issues

5.5.1.1 Is stationkeeping needed?

The addition of a large mirror and light shield to HST will increase the atmospheric drag resulting in faster decay of the orbit. The increased rate of orbital decay is likely to be in the range of a factor of two to three depending on the size and shape of the enhancement. This increase will likely require an interim re-boost mission (or missions) unless another solution is implemented. This analysis was to consider such an alternate solution to the accelerated orbital decay issue. In addition, a stationkeeping system may save a de-orbiting mission which would more than pay for itself.

The Analysis Issues, Design, and Discussion below are based on a readily available Ion Engine Stationkeeping System (IESS) currently in use on other missions.

5.5.1.2 Is the boost rate adequate

Is the boost rate of the proposed Ion Engine Stationkeeping System adequate to offset the decay rate for any arbitrary point in the solar cycle?

Model calculations show that the orbital-decay rate varies up to a maximum of 80 m/day at the nominal altitude of 600 km for the worst solar flux level, 250 J, whereas the boost rate capability of the proposed IESS is calculated to be between 500 and 700 meters per day when operating in the non-optimal-thrust mode described below. This provides adequate capacity to overcome significant altitude decay in a short period of time.

5.5.1.3 Is Science Efficiency adequate

Is the frequency of thrusting sufficiently low to allow reasonable science efficiency?

To maintain the spacecraft within 1% of its initial 600 km altitude, roughly 16 maneuvers will be required over the solar cycle (surprisingly invariant irrespective of the epoch chosen). At a boost rate of 600 meters per day, roughly 10 days are required for each maneuver while the interval between maneuvers varies from 28 months at solar cycle minimum to slightly less than 4 months at solar cycle maximum, thus providing an observing efficiency against stationkeeping always greater than 90%. For the assumed epoch of 2006, the first maneuver will be required in 27 months. This lead time quickly diminishes as the solar maximum approaches. For an epoch of 2008, the first maneuver is required after eight months.

5.5.1.4 Is there enough fuel

Is the fuel requirement reasonable to accomplish both mission phases; Stationkeeping and end-of-life ascent?

The fuel consumption was computed to achieve the assumed end-of-life altitude of 1000 km, which provides of the order of 1000 years of orbital "lifetime". Total ascent phase is of the order of 600 days. Approximately 120 Kgm of fuel is needed and, with approximately 2 Kgm required for each stationkeeping maneuver during the operational phase, a total fuel requirement of 160 Kgm is required for an active mission of 10 years.

5.5.2 Stationkeeping System Design

5.5.2.1 Problem

How to prolong the spacecraft mission lifetime with accelerated orbital decay, and to dispose of it safely at end-of-mission?

5.5.2.2 Concept

Use low-thrust ion engines to provide periodic stationkeeping for the spacecraft and, at end-of-mission, to boost the spacecraft to a sufficiently high orbit to meet the mandated debris removal requirement.

5.5.2.3 Assumptions

Schatten 2-sigma solar flux values

Spacecraft: Mass = 12,475 Kg
Cross sectional area = 90.5 sq. m

Orbital: Altitude = 600 km, circular
Stationkeeping window = 1% (6 km)
Inclination = 28.5 degree

Mission Initiation epoch = 2006 (not critical)

5.5.2.4 Conceptual Design

Redundant Hughes Xenon ion engine (ref.: 702 spacecraft series) or equivalent

Modular assembly attaches to FSS points

Power from J600 connector

Engines canted by 30 degrees from V1 axis in V1-V2 plane

During thrusting, V2 axis is normal to sun line and V1 axis is in plane of orbit

160 millinewton thrust; ISP = 3000 sec

Redundant 4.5 kW Power Supplies cross-strappped among engines

Power required during thrusting: 4.5 kW

5.5.3 Stationkeeping System Description

The concept for the proposed IESS is a modular design including two outboard plus back-up engines, their power supply, four pressurized Xenon vessels, power and fuel switching subsystems, and associated plumbing and wiring.

The structure on which the components are mounted attaches to the FSS mounting brackets on the aft shroud. The large diameter threaded hole in the existing HST trunnion sockets make ideal mechanical mounts for the ion thrusters. These trunnions are located and aligned to the HST vehicle center of mass, are

structurally stiff, and are not otherwise occupied. P601 is co-located with the starboard socket and circumference harnessing could route power to the other ion thrusters, bussed off of the first installation.

Ion Engine Stationkeeping System

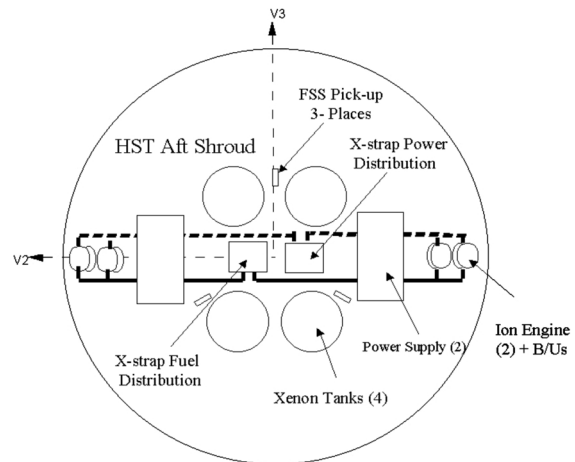


Figure 5.5 IESS Configuration

Approximately 4.5 kW are required to drive the engines at maximum thrust, however, the actual levels can be less. A non-optimized thrusting profile has been assumed to provide a worst case result. To simplify the analysis, the spacecraft is assumed to maintain a quasi-inertial attitude during thrusting rather than attempting to maintain the thrust vector normal to the orbital radius vector by a combination of slewing and rolling the spacecraft. The inertial attitude is such as to provide normal incidence for the solar arrays (appropriately rotated) in order to maximize their power generation. In this idealized, albeit inefficient case, one thruster is used at a time over 120 degrees of an orbit while the second operates for additional 120 orbital degrees. The computational model used allows no thrusting in either of the following conditions: 1) during eclipses in order to conserve battery power and 2) during any portion of the orbit when the scalar product of the thrust and velocity vectors becomes negative.

This section adapted from a report provided to the HST10X study by:
S. Sobieski, Swales Aerospace, July 1999.